12

A Bio-Robotic Toe & Foot & Heel Model of a Biped Robot for More Natural Walking: Foot Mechanism & Gait Pattern

Jungwon Yoon[1], Gabsoon Kim[2], Nandha Handharu[1] and Abdullah Özer[1]
[1]*School of Mechanical and Aerospace Engineering and ReCAPT*
Gyeongsang National University,
[2]*Control Instrumentation Engineering Department*
Gyeongsang National University,
Republic of Korea

1. Introduction

Humans possess a complex physical structure and can perform difficult movement tasks. Over the past few decades, many researchers around the world have concentrated on achieving human-like artificial mobility or dexterity either on humanoid robots or during the implementation of robotic assistive devices. In particular, humanoid-type robots mainly focused on hands to understand the mechanical and dynamical functions of ourselves. On the other hand, there have been few researches to achieve human like foot. Until now, human-like skillful mobility has not been achieved on humanoid robots, since the robotic feet are far from adaptation to keep stable contact on the ground and the current kinematic structures of a humanoid foot is different from that of a real human foot. Stability related issues have been the main goal for humanoid robots in relevant researches. Initially, humanoid robots were built so that they can walk stably with flat foot (Sakagani et al., 2002; Okada et al., 2004). These initial walking patterns were optimized for the highest stability, and the resulting walking pattern had knee bending and flat-feet walking. A more advanced strategy was developed for generating biped walking pattern involving heel strike and toe off motion in (Huang et al., 2001). However, because of the mechanism's limitation the knee bending walking patterns were always chosen for the benefit of stability, thus making it less natural. Today, more advanced control approaches, faster and more powerful actuators, and more sophisticated walking pattern generation strategies have helped the research goal to be shifted to pursue more natural walking patterns for biped robots, with the expectation that someday humanoid robot can coexist with human.

To improve walking capacity of humanoid-type robots, toe mechanisms with 1-dof was suggested earlier, (Ahn et al., 2003; Takahashi et al., 2004). For walking in a straight direction, 1-dof toe mechanism can supply faster walking for a robot. In addition, relative toe motion can increase the naturalness of robot walking and help to reduce the load on the knee joints, where high force and speed are required to achieve robot locomotion (Nishiwaki & Kagami, 2002). However, the foot device with 1-dof toe mechanism cannot

adapt turning during walking and may not satisfy safe and natural walking under uneven terrain conditions, (Takao et al., 2003). Takao et. al concluded through gait experiments that the robotic foot mechanisms with multi degree-of-motions can contribute smooth and effective body motions in the stance phase. A foot mechanism with such dexterous motions at toe, foot, and heel will certainly enable the humanoid robots to perform more efficient and skillful movements on various terrains. Therefore, it will be advantageous to develop foot mechanisms with multi-dof motions for humanoid-type robots to satisfy natural walking actions on various terrain situations. Even though serial actuations of rotary motors at foot joints can generate multi-dof motions, it is difficult to implement the active joints due to the high torque by the heavy humanoid weight. Thus, a serial-parallel mechanism can be a good solution to satisfy the desired performance of foot devices in humanoid robots since it can produce high rigidity, compactness, and precise resolution, as compared to serial mechanisms. In addition, the foot mechanism for humanoid-type robots should have multi-platforms to allow relative rotations between the toe and the foot, and to generate heel motions.

This chapter deals with a toe & foot& heel model that can allow a humanoid robot to walk more naturally, closer to a normal human. A foot device with a 4-DOF parallel mechanism is suggested to generate human-like foot motions. The mechanism for the toe & foot& heel motions for the humanoid consists of several toe platforms using a serial-parallel hybrid mechanism; a foot platform, a heel platform, corresponding limbs to the platforms, and the base, which is located at the humanoid shin. The suggested foot platform can generate pitch & roll motions at ankle position using 2-dof-driving parallel mechanism with two linear actuators fixed to the base. The toe and heel joint motions can be implemented by attaching 6-dof serial joints between the platform and the base, and by connecting the corresponding platform and the foot platform with a revolute joint. As a result, the suggested foot mechanism with more dexterous functions can adjust the biped robot's walking movements during the stance phase of gait. Together with its design advantage, the suggested toe, foot, and heel model can also facilitate more natural walking patterns for biped robots. A new alternative methodology to generate gait pattern online with knee stretched motion utilizing toe and heel joints will also be presented within this chapter.

2. The mechanism description

2.1 Human foot

The set of foot and ankle is mechanically very complex since it has 26 bones, 33 joints, more than 100 muscles, tendons, and ligaments (Guihard &Gorce, 2004). All these mechanical elements collaborate to offer the body support, balance, and mobility. Structurally, the foot has three main parts: The hindfoot, the midfoot, and the forefoot. The hindfoot is composed of three joints and connects the midfoot to the ankle. It lets the foot to move up and down (-50°- 20°) and provides slight rotations. The midfoot has five irregular shaped tarsal bones, which acts as a shock absorber. The forefoot has five phalanges of toes and their connecting long bones called metatarsals. Their maximum rotation range is about 90° when the toes are totally raised.

2.2 Mechanism description for toe, foot, and heel models

The mechanism for the toe & foot & heel motions of the humanoid robot consists of several toe platforms, a foot platform, and a heel platform and corresponding limbs to the

platforms, revolute joints between the toes and the foot platform, and a revolute joint between the heel and the foot platform as shown in Figure 1. Base of each platform is located at a humanoid shin.

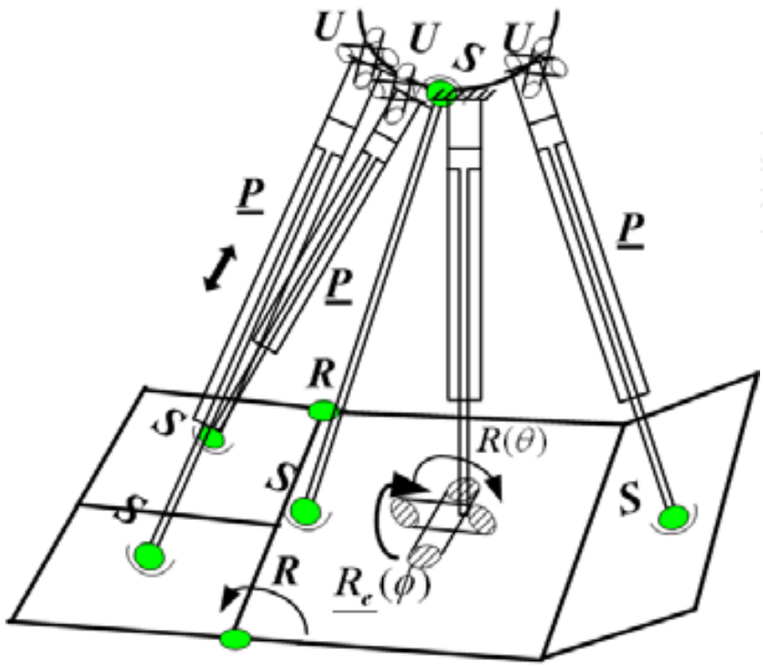

Fig. 1. A novel foot mechanism with toe, foot, and heel motions

In the figure, the letters *P*, *R*, *U*, and, *S* represent prismatic, revolute, universal, and spherical joints, respectively. An underlined letter represents an actuated joint. The numbers of toe and heel joint are selected as two and one, respectively. One limb with 6-dof serial joints (S-P-U) is attached to toe and heel platforms, respectively, while middle limb ($\underline{P_e}$-$\underline{R_e}$-*R*) and four-bar limb (S-S) are attached to the foot platform. The middle limb with equivalent 3-dof serial joint ($\underline{P_e}$-$\underline{R_e}$-*R*) is driven by the 2-dof driving mechanism that is equivalent active serial prismatic and revolute joints ($\underline{P_e}$-$\underline{R_e}$) with two base-fixed prismatic actuators. The four-bar limb will allow the foot platform to generate a pitch motion (θ) according to active prismatic joint motions ($\underline{P_e}$) of the 2-dof driving mechanism. In result, the foot platform can generate two rotations with equivalent 2-dof serial joint ($\underline{R_e}$-$\underline{R_e}$). A toe joint motion can be implemented by attaching 6-dof serial joints (*S*-$\underline{P}$-*U*) between the toe platform and the base, and by connecting the toe and the foot platform with a revolute joint. Similarly, a heel joint motion can be implemented by attaching a 6-dof serial joints (*S*-$\underline{P}$-*U*) limb and a revolute joint to the rear part of the foot platform

Since toe and heel platforms have one limb with one 6-dof serial joint (*S*-$\underline{P}$-*U*) and the foot platform has 2-dof serial joint ($\underline{R_e}$-$\underline{R_e}$), the final output displacement of each platform is dependent only on that of the foot platform with its 2-dof serial joint ($\underline{R_e}$-$\underline{R_e}$), which is the intersection of the special Plücker of two limbs. Therefore, the suggested mechanisms have five degrees of freedom in total when the toe joints are two and the heel joint is one. The suggested foot model can generate pitch & roll motions at the ankle position of a humanoid robot, toe joints motions, and a heel joint motion. Toe joint motions can be extended by attaching another toe platform with an additional 6-dof limb to the foot platform.

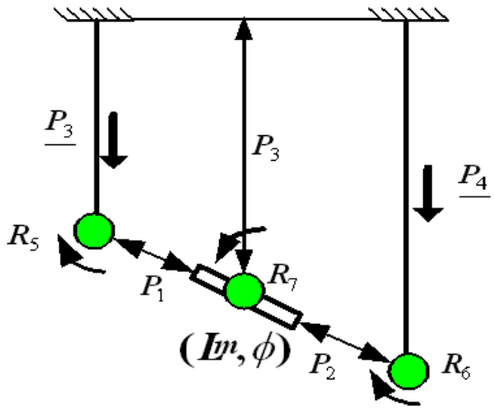

(a) T-R type joint array

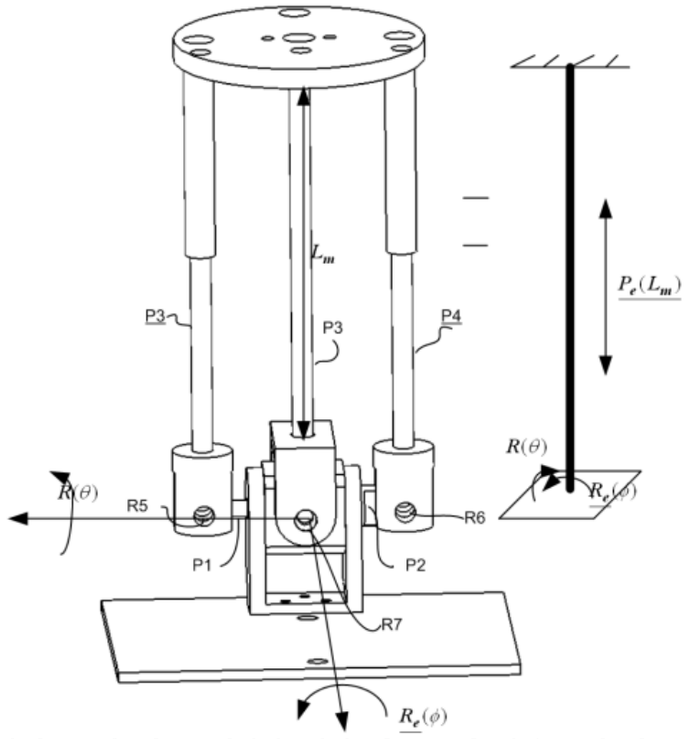

(b) T-R type Implementation

Fig. 2. T-R type 2-dof-driving mechanism

Figures 2 shows a T-R type 2-dof driving mechanism that can generate 2-dof translational and rotational motions of the platform using two base-fixed prismatic actuators. Figure 2(a) shows the joint array of the T-R type 2-dof-driving mechanism. The T-R-type driving mechanism consists of passive prismatic joints (P_1 and P_2) between revolute joints (R_5 and R_6) at the upper ends of the active prismatic joints ($\underline{P_3}$ and $\underline{P_4}$) fixed to the base and end-effector of the driving mechanism, and includes a passive prismatic joint (P_3) between the revolute joint R_7 of the end-effector and base plate. P_3 allows the end-effector to move in the z-direction only and R_7 allows the end-effector to rotate about the y-axis only. A CAD model

of the T-R-type driving mechanism is shown in Figure 2(b). Consequently, the T-R-type driving mechanism is conceptually equivalent to active serial prismatic and revolute joints ($\underline{P_e}$-$\underline{R_e}$). Also, R-R-type mechanism will be generated by attaching an additional rotation bar, which will change a translation motion to a rotation as shown in Figure 3.

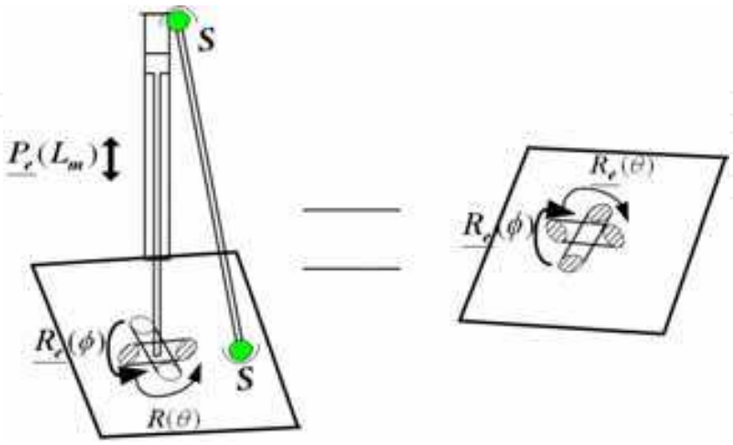

Fig. 3. R-R type 2-dof driving mechanisms

Figure 4 shows the link-pair relationship diagram for the 2-dof-driving mechanism. The white boxes represent passive joints and the hatched boxes represent active joints. Lines between letters represent links. It is possible to consider each driving mechanism as equivalent to the two actuated joints ($\underline{P_e}$-$\underline{R_e}$ *or* $\underline{R_e}$-R_e) in terms of the number and type of degrees of motion. The motions of the given mechanism can be verified using Grübler's formula as:

$$M = d(n-g-1)+\sum_{i=1}^{g} f_i \tag{1}$$

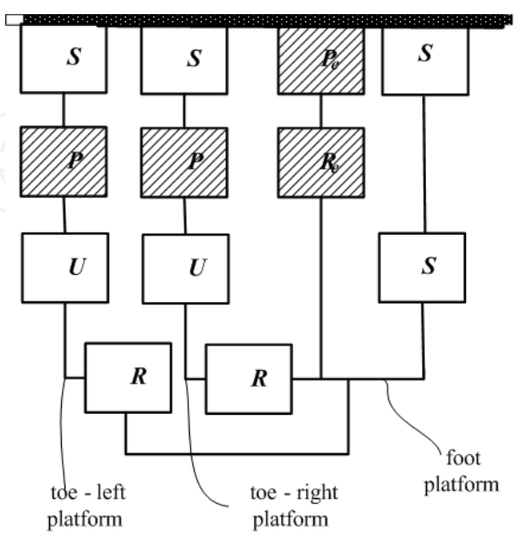

Fig. 4. The link-pair relationship diagram of the 4-dof mechanisms with three platforms

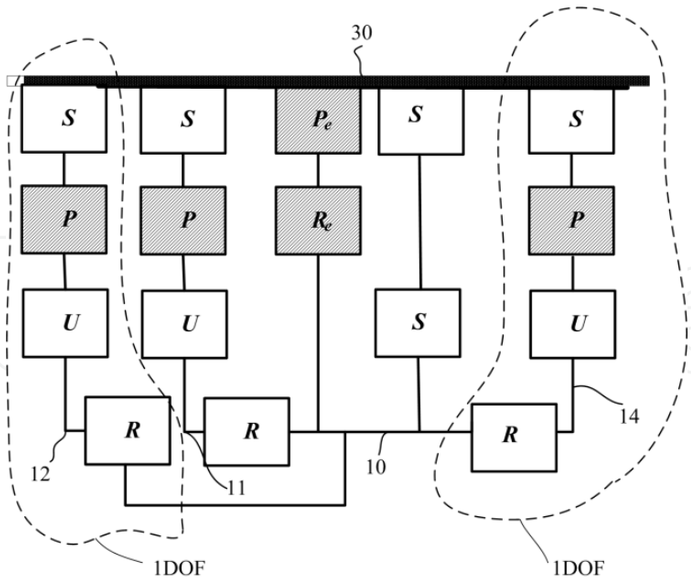

Fig. 5. The joint structure of the mechanism with the N+2 DoF

If the driving mechanisms are considered equivalent to serial ($\underline{P_e}$-$\underline{R_e}$) joints and the number of the toe platform and the heel platform is two and zero, the mobility of the 4-dof mechanisms with three platforms as shown in Figure 4 is:

$$M_{4dof} = 6(10 - 12 - 1) + 1\times 6 + 2\times 2 + 3\times 4 = 4$$

The Figure 5 shows that the numbers of the toe platform and the heel platform with the foot platform determine the mobility of the mechanism. If the platform numbers is N except the foot platform, then, the mobility of the mechanism can be computed as;

$$\begin{aligned} M_{(2+N)dof} &= 6((4+3N)-(4+4N)-1)+1\times 2N + \\ &2\times N + 3\times(2+N) + 3\times(2+N) = 2+N \end{aligned} \tag{2}$$

Therefore, the mobility of the mechanism can be generalized as follows:

$$M = 2 + N$$

where M is the mobility of the suggested mechanism and N is the number of platforms with a 6-joint (S-$\underline{P}$-U) limb and a revolute joint. For example, If N=3, the mobility becomes five as follows;
When N=3,

$$M_{(2+3)dof} = 6(13 - 16 - 1) + 1\times 8 + 2\times 3 + 3\times 5 = 5$$

Figure 6 shows that when N=3, the mechanism can generate two toe joints motions and foot motions with two rotations and one heel joint motion.
Figure 7 shows the developed humanoid foot which can generate pitch motions of the two toe platforms and the heel platform with relative rotations between the corresponding platform and the foot platform. The mechanism can generate two rotations at an ankle with a $\underline{R}$-$\underline{R}$ type 2-dof-driving mechanism motion.

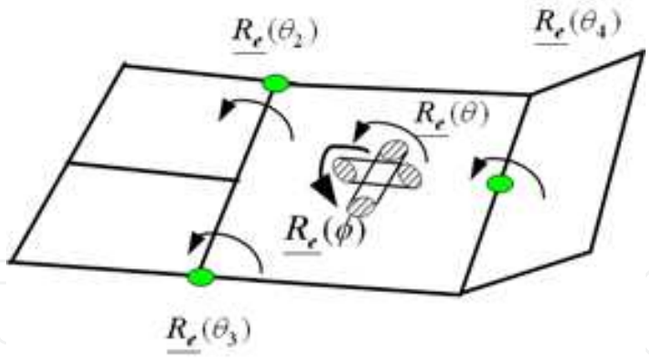

Fig. 6. Platform motions with N=3

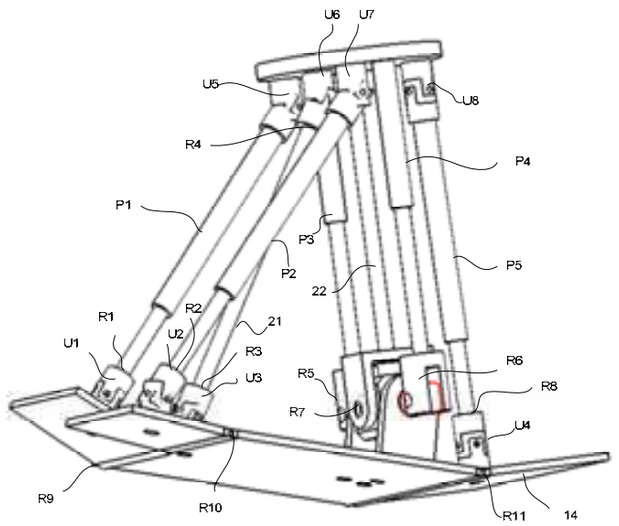

Fig. 7. The developed humanoid foot

3. Walking simulations with a biped robot

3.1 Kinematics of a biped robot with the foot models

The kinematic relationships of a biped robot with the foot models are derived to generate walking trajectory. Forward and inverse kinematic equations are used to calculate the posture of robot and angles of each joint. Coordinate system of the biped robot with foot models with two toe joints and one heel joint is shown in Figure 8. The base coordinates $\{\boldsymbol{O_b}\}$ is located on the ground in the middle point of the feet, and the truck coordinates $\{\boldsymbol{O_M}\}$ is located on the middle point of waist. The left $\{\boldsymbol{O_{f,L}}\}$ and right $\{\boldsymbol{O_{f,R}}\}$ foot coordinates are located on the foot platform. The waist coordinate $\{\boldsymbol{O_w}\}$ is located on the upper position of each limb.

The inverse kinematics computes angles $\phi_{1,i}, \theta_{2,i}, \theta_{3,i}, \theta_{4,i}, \phi_{5,i}, \nu_{6,i}$ of each joint of the biped robot given the position and orientation of the waist center, and the toe joints $\theta_{tr,i}, \theta_{tl,i}$ and the heel joint $\theta_{h,i}$, where $\phi_{1,i}, \theta_{2,i}, \theta_{3,i}$ are pitch and roll angles of the ankle joint, knee joint angle, respectively. $\theta_{4,i}, \phi_{5,i}, \nu_{6,i}$ are the joint angles of the pelvis, and i is the sub-suffix for left L and right R. For inverse kinematics of the biped robot, the equation can be derived as follows;

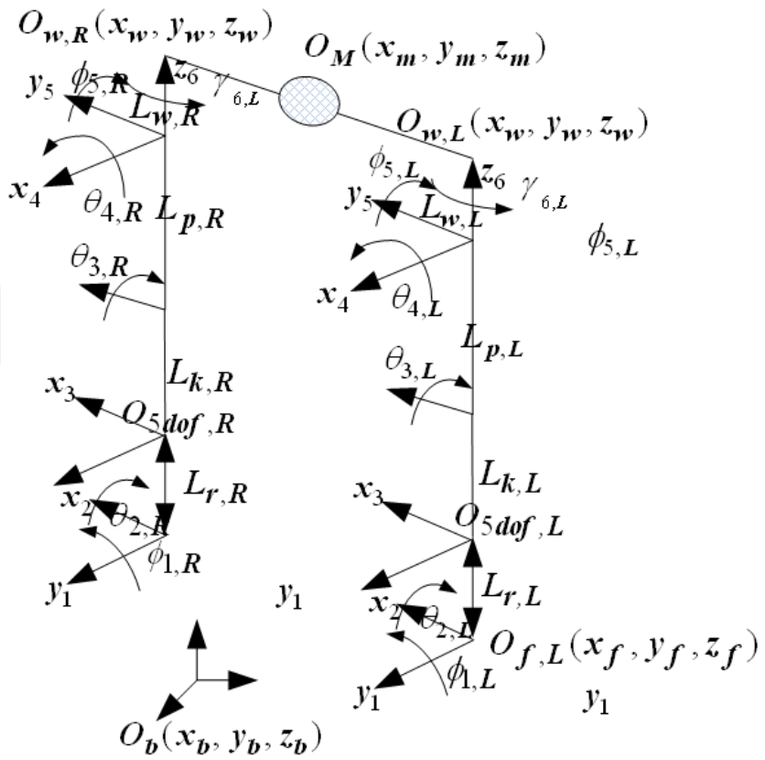

Fig. 8. Coordinate system of the biped robot

$$O_{t,i} = R_y(\phi_{1,i})R_x(\theta_{2,i})T_f^3(0,0,L_{k,i}+L_{r,i})$$
$$R_x(\theta_{3,i})T_3^4(0,0,L_{p,i})R_x(\theta_{4,i})R_y(\phi_{5,i})T_5^w(0,0,L_w)$$

$$(\boldsymbol{i} = \boldsymbol{L}, \boldsymbol{R}) \tag{3}$$

where $O_t(x_t, y_t, z_t)$ is the vector from the foot coordinate $O_{f,i}$ to waist coordinate $O_{w,i}$, and L_r, L_k, L_p, and L_w are the average length of the 2dof driving mechanism, the length of calf, thigh, and waist, respectively. $\boldsymbol{R}$ is the rotation matrix, $T_f^3(x,y,z)$ is the translation matrix from local reference frame $\boldsymbol{O}_f$ (x_f, y_f, z_f) of the foot platform to the 3-axis mobile reference frame $\boldsymbol{O}_3$ (x_3, y_3, z_3). If $L_{w,i}$ is equal to zero, then the equation (3) can be simplified into equation (4)

$$x_t = (-\sin(\phi_1)\sin(\theta_2)\sin(\theta_3) + \sin(\phi_1)\cos(\theta_2)\cos(\theta_3))L_p + \sin(\phi_1)\cos(\theta_2)L_{kr} \tag{4-a}$$

$$y_t = (-\cos(\theta_2)\sin(\theta_3) - \sin(\theta_2)\cos(\theta_3))\mathrm{L_p} - \sin(\theta_2)L_{kr} \tag{4-b}$$

$$z_t = (-\cos(\phi_1)\sin(\theta_2)\sin(\theta_3) + \cos(\phi_1)\cos(\theta_2)\cos(\theta_3))\mathrm{L_p} + \cos(\phi_1)\cos(\theta_2)\mathrm{L_{kr}} \tag{4-c}$$

From the equations (4-a) and (4-c), the roll angle ϕ_1 of ankle joints can be computed as;

$$\phi_1 = \tan^{-1}(x_t / z_t)$$

From the equation (4-b) and equation (4-c), the equation (5) can be derived by deleting the parameter θ_3 and utilizing the MATLAB symbolic toolbox (Mathworks).

$$\begin{aligned} f_1 = & (y_t \cos(\phi_{1,i}) \sin(\theta_2) - \cos(\theta_2) z_t - (L_k + L_r) \\ & \cos(\phi_1))^2 - (-\cos(\phi_1)^2 y_t^2 \cos(\theta_2)^2 - 2\cos(\phi_1)\cos(\theta_2) \\ & y_t z_t \sin(\theta_2) - z_t^2 + z_t^2 \cos(\theta_2)^2 + \cos(\phi_1)^2 L_p^2) \end{aligned} \quad (5)$$

Then, the kinematic relationships of the 5-dof foot mechanism are shown in Figure 9. A local reference frame for the foot platform, $\boldsymbol{O}_f(x_f, y_f, z_f)$, is located at the center of the foot platform. A local reference frames for the toe-left $\boldsymbol{O}_f$ (x_f, y_f, z_f) and the toe-right $\boldsymbol{O}_{tr}$ (x_{tr}, y_{tr}, z_{tr}) are centered at each toe platform, respectively. The base of the 5-dof foot mechanism, $\boldsymbol{O}_{5dof}$ $(x_{5dof}, y_{5dof}, z_{5dof})$, mobile reference frames is located on the z-axes of reference frame $\boldsymbol{O}_f$ of its platform. b is the distance of y-axis from center position $\boldsymbol{O}_f$ of the foot platform to the toe-revolute joint, a is the distance of y-axis from the revolute joint to center position $\boldsymbol{O}_{tl}$ of the toe platform, and c is the distance of x–axis from the foot platform joint to center position $\boldsymbol{O}_{tl}$ of the toe platform .

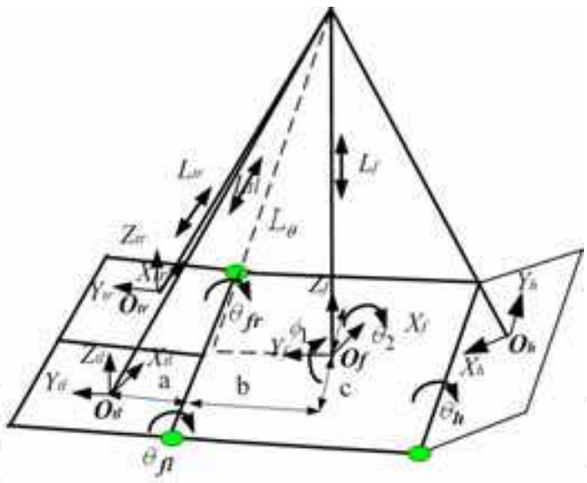

Fig. 9. The kinematic model of the foot mechanism

The height L_f from the foot reference frame to $\boldsymbol{O}_{5dof}$ reference frame have following relation

$$L_\theta^2 = b^2 + L_f^2 - 2bL_f \cos(\theta_2 + \pi/2) \quad (6)$$

where L_θ is a constant distance value from center revolute joint to $\boldsymbol{O}_{5dof}$ reference frame. From equation (6), the height L_f can be computed as

$$L_f = -b\sin(\theta_2) + \sqrt{b^2 \sin(\theta_2)^2 - b + L_\theta^2} \quad (7)$$

Then, the equation (7) can be rearranged into equation (8).

$$f_2 = b^2 + (L_f)^2 - 2bL_f\cos(\theta_2 + \pi/2) - L_\theta^2 \tag{8}$$

Since the equations (5) and (8) have only unknown parameters of θ_2 and L_f, these two nonlinear equations can be solved by Newton-Rapson's numeric method. If the parameter θ_2 and L_f are solved, then θ_3 can be computed by utilizing the equation (4-c). Next, the lengths of the actuators of the 2-dof driving mechanism are then obtained as:

$$L_{f1} = L_f + \frac{L_{base}\tan\phi}{2} \quad L_{f2} = L_f - \frac{L_{base}\tan\phi}{2} \tag{9}$$

where L_{f1}, L_{f2}, and L_{base} are the active lengths of the left and right actuators, and the distance between the two active prismatic joints of the 2-dof mechanism, respectively.
If the toe joint angles θ_{tr}, θ_{tl} and the heel joint angle θ_h are given, the actuator's length of each platform can be computed as follows;

The mobile reference frame $\boldsymbol{O}_{5dof}$ can be represented in the base reference frame (X_b, Y_b, Z_b) as:

$$O_{5dof} = O_f + R_y(\phi_1)R_x(\theta_2)T_f^{5dof}(0,0,L_f) \tag{10}$$

The coordinate position $\boldsymbol{O}_{tl}$ of the toe-left mobile reference frame can be represented in the base reference frame (X_b, Y_b, Z_b) as:

$$\begin{aligned} O_{tl} &= R_y(\phi_1)R_x(\theta_2)T_r^m(-c,b,0) \\ &+R_y(\phi_{1,i})R_x(\theta_{2,i})T_m^{tl}(0,a,0) \end{aligned} \tag{11}$$

Similarly, the coordinate position $\boldsymbol{O}_{tr}$ of the toe-right mobile reference frame can be represented in the base reference frame (X_b, Y_b, Z_b) as:

$$\begin{aligned} O_{tr} &= R_y(\phi_1)R_x(\theta_2)T_r^m(c,b,0) \\ &+R_y(\phi_{1,i})R_x(\theta_{2,i})T_m^{tl}(0,a,0) \end{aligned} \tag{12}$$

Subsequently, the toe-left actuator length can be easily computed as follows;

$$L_{tl} = \sqrt{|O_{tl} - O_a|} \tag{13}$$

Also, the toe-right actuator length can be easily computed as follows;

$$L_{tr} = \sqrt{|O_{tr} - O_a|} \tag{14}$$

Using the above method, the heel actuator length can be computed as follows;

$$L_h = \sqrt{|O_{heel} - O_a|} \tag{15}$$

3.2 The models of normal gait cycle

Normal gait is defined as series of rhythmic alternating movements of the limbs and trunk (Perry, 1992). The gait cycle is the activity that occurs between heel strike by one extremity and the subsequent heel strike on the same side. The gait cycle consists of stance and swing phases. The entire period during which the foot is on the ground is the stance phase. Conversely, during the swing phase, the foot that is stepping forward is not in contact with any object. Stance phase accounts for approximately 60% of a single gait cycle, while swing phase accounts for approximately 40%. During the stance phase, the human foot performs a rolling motion on the ground. Throughout the motion trajectory, one foot lands on its heel at some heel-strike angle a (loading phase). Then, the foot stays flat on the ground during mid-stance (mid-stance phase). After the sole of the foot has made contact with the ground, the heel begins to rise from the ground with relative rotation at the metatarsal joint, and the contact moves to the toe with a toe-off angle λ (terminal stance). Finally, the sole of the foot flattens before the foot is lifted from the ground (pre-swing phase). To simulate these foot trajectories on a planar surface during stance phase, the platform variables θ_f and θ_r of the footpad mechanism can be defined for each subphase during the stance phase, as shown in Figure 10. Note that the left and right toe joints are identical and during loading phase, the toe joint angle θ_t and the foot pitch angle θ_f are identical, while the foot pitch angle θ_f and the heel joint angle θ_h are identical during terminal stance

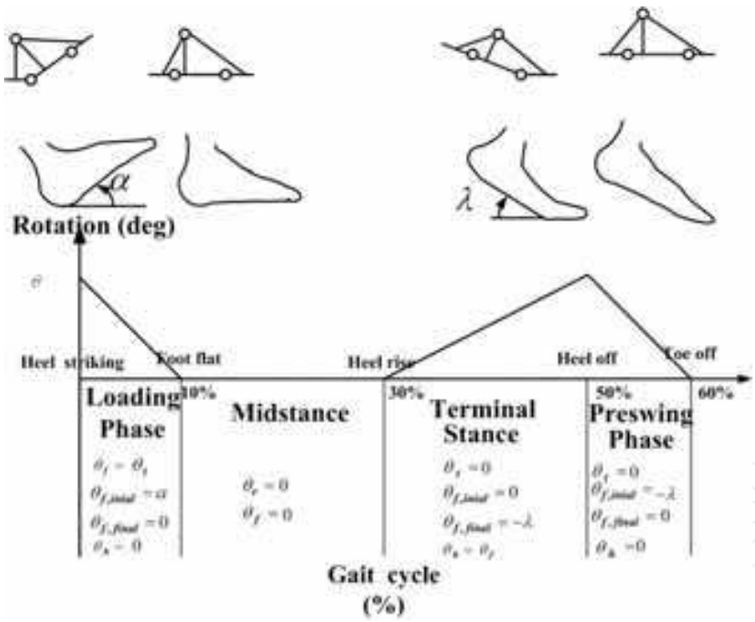

Fig. 10. Foot trajectory during stance phase

3.3 Trajectory generation of the humanoid robot with the suggested toe, foot, and heel models

If heel-strike angle α, toe-off angle λ, step length are 20°, and 30cm, the foot trajectory configuration at a planar surface with respect to the gait cycle is obtained as shown in Figure 11. These simulations based on gait analysis showed that the suggested mechanism with toe, foot, and heel models can generate natural foot motions, including relative rotations at the toe and the heel during the stance phases.

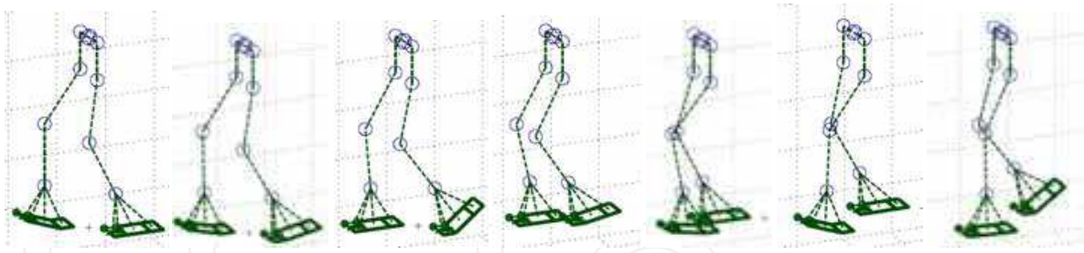

(a) (b) (c) (d) (e) (f) (g)

Fig. 11. The walking simulations of a biped robot with toe, foot, and heel models during the stance phase

4. Online gait pattern generation

Traditionally, the ZMP based trajectory method was used by researchers to generate gait patterns for humanoid robots. Approaches using simplified biped robot model such as rolling mass model or inverted pendulum model were usually being utilized to solve the ZMP equations, (Nishiwaki et al., 2002). However, there could be difficulties in some cases to achieve the necessary high hip accelerations to realize the desired ZMP trajectories. In such cases, since the trunk has the biggest mass value, energy consumption increases, and control for task execution of the upper limbs becomes difficult, (Huang et al., 2001). Moreover, no matter how well the algorithm can make the biped robot follow the desired ZMP trajectory, the motion result of the hip itself cannot be assured. This has motivated several researchers to find alternative ways of generating gait patterns for biped robots. Huang et al. proposed a gait pattern algortihm that control the hip motion with adjustable hip parameters that achieved highest stability margin, instead of designing the ZMP trajectory first. This way, the motion result can be directly controlled with those parameters. Though Huang's method has some advantages compared to the ZMP trajectory method, it required an optimization scheme to select best hip parameters that can obtain gait pattern with the highest stability margin which made the algorithm unable to generate the gait pattern online. Advancement has been made with this method, (Peng et al., 2004). However, since typical walking pattern has to be defined first, there will be limitation on the variety of the gait patterns. Hence, it is very important to improve effective gait pattern algorithms.

In terms of foot mechanism more important developments were made as discussed in (Ramzi et al., 2003; Nishiwaki et al., 2002; Yoon et al., 2007; Ki Ahn et al., 2003). These robots had modified feet using extra joints in their toe positions. There are many researches concerning toe joints in the biped robot research. Faster walking, longer steps and more degrees of freedom were obtained in these research studies. Knee stretch motion has often been related to the naturalness of biped walking. Recently some researchers tried to achieve stable walking patterns involving knee stretch motion (Kurazume et al., 2005; Ogura et al., 2006). There is even a commercial product for humanoid robot that is able to walk with straight knee (Garage, 2008). The research utilized a conventional biped robot with flat foot to generate straight walking pattern (Kurazume et al., 2005). One of the main reasons why knee stretch motion for biped walking is hard to achieve is that during the knee stretch, the inverse kinematics solution for the leg becomes singular. This research has not been able to avoid this singularity and utilized "if-then" commands on its algorithm. In (Ogura et al., 2006), the researchers tried to achieve knee stretch walking by adding extra joint in the

humanoid robot. In this way the singularity can be overcome by the extra joint in the waist owing to losing some DOF in the knees. To achieve knee stretch walking pattern, we will attempt to add extra joint in the heel here. It is true that human doesn't have heel joint, but gait analysis research shows that human walking sequence has heel strike motion and the knee stretch occurs during this phase of walking (Perry, 1992). During this motion, human heel acts as an extra support region. Based on these facts, we decided to add extra heel joint to produce some support region. Figure 12 shows the sequence of foot support areas during stance phase. With the extra heel joint, we propose a walking pattern strategy that enables the knee stretch motion which can avoid singularity. The loss of degree of freedom in the knee can be overcome through the existence of the heel joint. Our algorithm can generate stable knee stretch walking patterns without singularity. With knee-stretched motion, biped robot walking pattern will not only become more similar to human, but also will require less torque and thus making the pattern more energy efficient as human walking itself is optimized to energy efficiency (Kurazume et al., 2005; Ogura et al., 2006). Moreover, with our proposed mechanism, utilizing extra addition of heel joint is comparably less sophisticated than those biped robots, which have waist joints. We studied our algorithm with a biped robot in computer simulation. The walking trajectory generated through this method has successfully generated knee stretch walking patterns. Because of the addition of the heel joints, not only the support area during double support phase was increased, but singularity during the knee stretch motion has been also avoided. As the computer simulation results, the proposed gait pattern has showed better performance compared to the common walking gait in terms of joint torque requirements and energy consumptions.

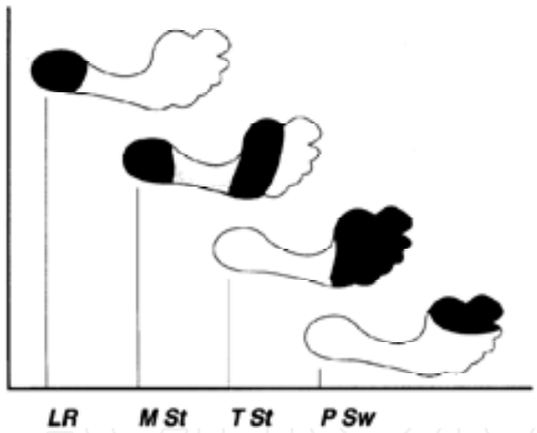

Fig. 12. Human sequence of foot support areas during stance phase (Perry, 1992).

4.1 Biped robot model and walking cycle

The suggested biped robot model has 5 degrees of freedom in each leg, with the extra 2 DOF coming from the toe and heel joints. The center of mass in each link is considered to be right in the center of each link. The biped configuration is shown in Figure 13. Biped walking is a periodic phenomenon. A complete walking cycle is composed of double-support phase and single support phase. The cycle starts from the beginning of the double support phase, where the heel strike motion occurs, and ends after the swing leg finishes its swing phase. Figure 13 also shows a complete walking cycle along with the biped configuration. The walking pattern that we discuss in this chapter covers only the motion in the sagittal plane.

Given the foot and hip trajectories, toe-heel and knee trajectories were obtained from the kinematic constraints of the mechanism.

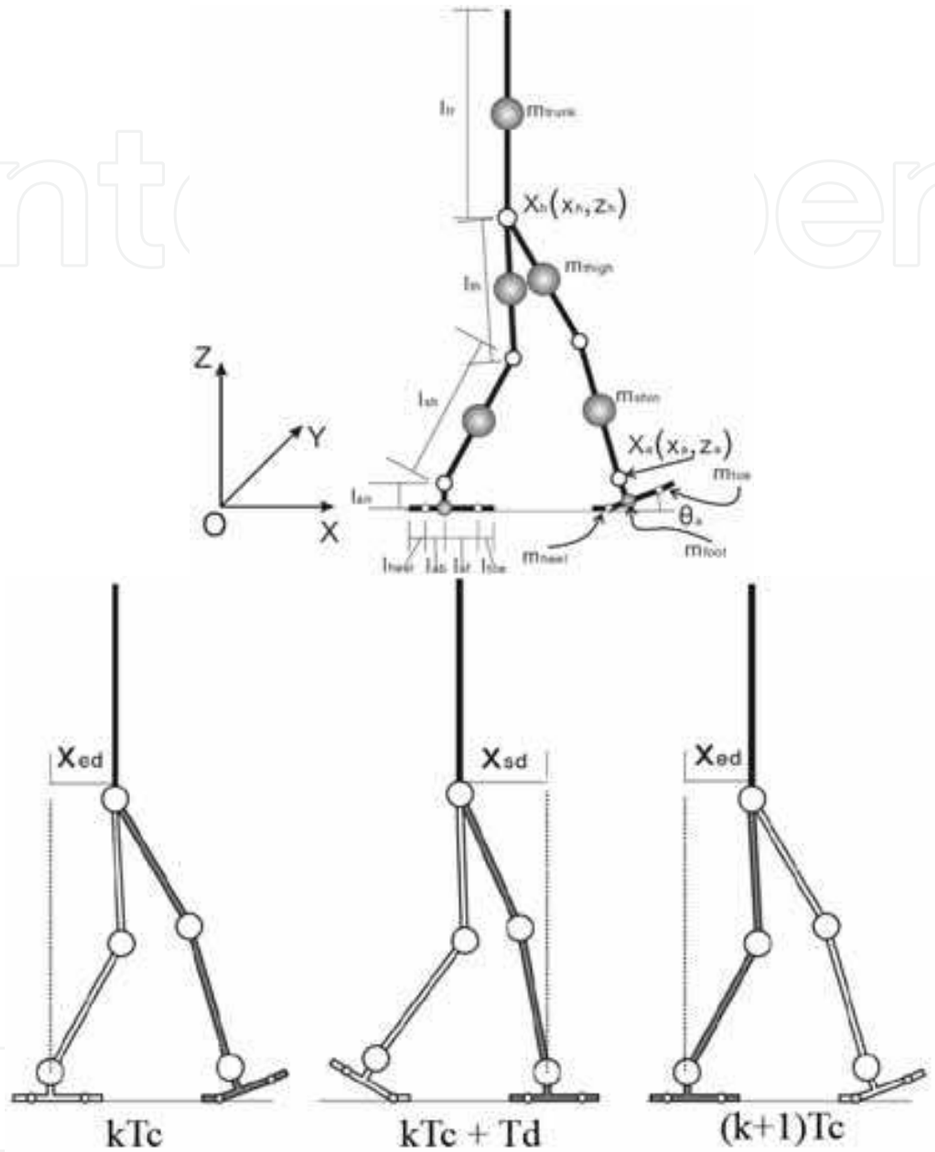

Fig. 13. Model of the biped robot and a complete walking cycle.

4.1.1 Initial foot trajectory

We planned for the initial foot trajectory as mentioned in (Huang et al., 2001). In sagittal plane each foot trajectory can be represented by vector $X_a = [x_a(t), z_a(t), \theta_a(t)]^T$, where $(x_a(t), z_a(t))$ is the coordinate of the ankle, and $\theta_a(t)$ denotes the angle between the foot and the x-axis. A similar vector can also denote the toe and heel trajectories. For toe $X_{toe} = [x_{toe}(t), z_{toe}(t), \theta_{toe}(t)]$, where $(x_{toe}(t), z_{toe}(t))$ is the coordinate of the toe, and $\theta_{toe}(t)$ denotes the angle between the toe and the foot. And, for heel $X_{heel} = [x_{heel}(t), z_{heel}(t), \theta_{heel}(t)]$, where $(x_{heel}(t), z_{heel}(t))$ is the coordinate of the heel, and

$\theta_{heel}(t)$ denotes the angle between the heel and the foot. Figure 14 shows the detailed configuration of each vector of the links in the foot.

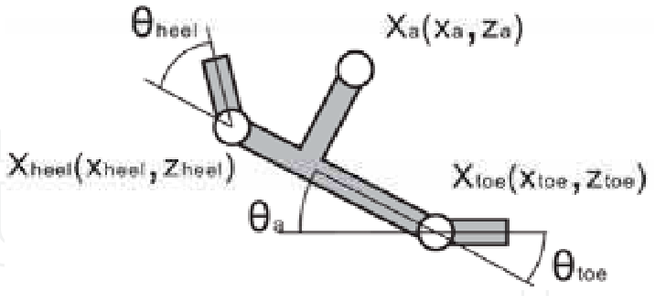

Fig. 14. Link vector configuration of the biped foot

The foot trajectory can be expressed by the function with respect to time, with a walking period of T_c , as

$$x_a(t) = \begin{cases} kD_s, & t = kT_c \\ kD_s + l_{an}\sin q_b + \cdots & \\ \quad l_{af}(1-\cos q_b), & t = kT_c + T_d \\ kD_s + L_{ao}, & t = kT_c + T_m \\ (k+2)D_s + l_{an}sinq_f - \cdots & \\ \quad l_{ab}(1-cosq_f), & t = (k+1)T_c \\ (k+2)D_s, & t = (k+1)T_c + T_d \end{cases}$$

$$z_a(t) = \begin{cases} l_{an}, & t = kT_c \\ l_{af}\sin q_b + l_{an}\cos q_b, & t = kT_c + T_d \\ H_{ao}, & t = kT_c + T_m \\ l_{ab}\sin q_f + l_{an}\cos q_f, & t = (k+1)T_c \\ l_{an}, & t = (k+1)T_c + T_d \end{cases} \quad (16)$$

$$\theta_a(t) = \begin{cases} 0, & t = kT_c \\ q_b, & t = kT_c + T_d \\ q_f, & t = (k+1)T_c \\ 0, & t = (k+1)T_c + T_d \end{cases}$$

where T_c, T_d, T_m are the period of one walking step, double support phase, and when the foot at the maximum height respectively. L_{ao} and H_{ao} are the x and z positions of the foot when it reaches the highest position , q_b and q_f are the initial toe off and heel strike angles respectively. While the vector position of the toe and heel will always be at the tip of the foot, the angle trajectories of the toe and heel are not the same as the foot. The toe and heel trajectories were designed so that it will land parallel with the ground, they can be expressed as

$$\begin{bmatrix} x_{toe}(t) \\ z_{toe}(t) \end{bmatrix} = \begin{bmatrix} x_a(t) \\ z_a(t) \end{bmatrix} + R_y(\theta_a(t)) \begin{bmatrix} l_{af} \\ -l_{an} \end{bmatrix}$$

$$\begin{bmatrix} x_{heel}(t) \\ z_{heel}(t) \end{bmatrix} = \begin{bmatrix} x_a(t) \\ z_a(t) \end{bmatrix} + R_y(\theta_a(t)) \begin{bmatrix} -l_{ab} \\ -l_{an} \end{bmatrix}$$

$$\theta_{toe}(t) = \begin{cases} 0, & t = kT_c \\ -q_b, & t = kT_c + T_d \\ 0, & t = (k+1)T_c \end{cases} \quad (17)$$

$$\theta_{heel}(t) = \begin{cases} 0, & t = kT_c \\ -q_f, & t = kT_c + T_d \\ 0, & t = (k+1)T_c \end{cases}$$

where R_y is the rotation matrix about y axis. To ensure the continuity of the trajectories, a third order cubic spline interpolation is implemented for each trajectory for generating continuous trajectory function.

After the initial foot, toe and heel trajectories are obtained, the support area of the stable margin througout the whole walking cycle can also be determined. This has been used later on as the base of the ZMP trajectory definition. Using this strategy, the increment of the support area during double support phase compared to the walking pattern without utilizing toe and heel joints can be shown. Figure 15 shows the difference between both the cases.

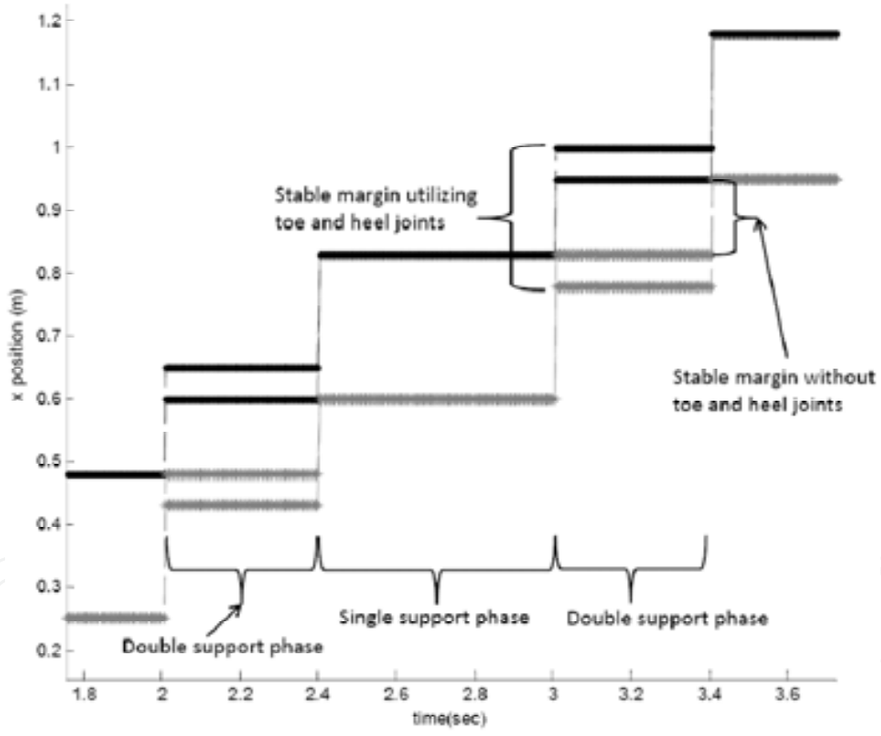

Fig. 15. Comparison of support area

4.2 Online trajectory generation

4.2.1 Desired ZMP trajectory and CoM trajectory

Zero moment point (ZMP) is the main criterion in biped robots for stable walk. We defined the ZMP trajectory after obtaining the support area. We chose moving ZMP trajectory instead of a fix one. The ZMP slides from one stable point to another stable point in each of the phases of the walking sequence. The ZMP trajectory can be expressed as

$$p_x(t) = \begin{cases} m_1(t-t_1)+x_1, & kT_c < t < kT_c + T_d \\ m_2(t-t_3)+x_3, & kT_c + T_d t < t < (k+1)T_c \end{cases}$$

$$\begin{aligned} &m_1 = \tfrac{x_2-x_1}{t_2-t_1}, && m_2 = \tfrac{x_4-x_3}{t_4-t_3}, \\ &t_1 = (k+1)T_c, && t_2 = (k+1)T_c + T_d, \\ &x_1 = kD_s + l_{af} + (l_{toe}/2), && \\ &x_2 = (k+1)D_s - l_{ab} - (l_{heel}/2), && \\ &t_3 = (k+1)T_c + T_d, && t_4 = (k+2)T_c, \\ &x_3 = (k+1)D_s - l_{ab} - (l_{heel}/2), && \\ &x_4 = (k+1)D_s + l_{af} + (l_{toe}/2), && \end{aligned} \tag{18}$$

where p_x is the ZMP position in x direction.
The center of mass (CoM) trajectory was obtained by solving a differential equation from the simplified model of the biped robot as mentioned in (Choi et al., 2007). The ZMP equation was expressed as

$$p_x = c_x - (1/\omega_n^2)\ddot{c_x} \tag{19}$$

where $\omega_n \cong \sqrt{g/c_z}$ is the natural frequency of the simplified biped walking robot system, (c_x, c_z) is the vector position of CoM and g is the value of gravity. By solving (19) with respect to (18), the x trajectory of CoM (c_x) will be obtained. In our method we keep the center of mass (CoM) trajectory at a fix height, thus the z trajectory of CoM (c_z) is fixed. The hip trajectory will be determined from the CoM trajectory as

$$\begin{aligned} x_h(t) &= c_x(t), \\ z_h(t) &= c_z(t) - (l_{tr}/2) \end{aligned} \tag{20}$$

where $(x_h(t), z_h(t))$ is the vector position of the hip.

4.2.2 Hip trajectory

The hip trajectory obtained by the above method can indeed satisfy the desired ZMP trajectory mentioned in (18) for simplified model of the biped robot. But once we apply the trajectory for the complete system of biped robot, the limited hip motion has caused the non capability of the trajectory to achieve all of the desired ZMP trajectory.
The parameterization of the hip trajectory mentioned in (Huang et al., 2001) is applied to make the adjustments. The only difference from (Huang et al., 2001) is that we utilize the parameter value x_{ed} and x_{sd} from the previous hip trajectory obtained above. In this way, no optimization scheme needs to be used. Those parameters are used to generate new hip trajectory by the same method of interpolation. And, since those parameters obtained from an already stable trajectory, we can also guarantee the stability of the new hip trajectory. Figure 16 shows the difference between adjusted CoM trajectory and the initial one.
After the hip trajectory is decided, the knee trajectory is decided by the inverse kinematics formula. Thus, all links trajectories are determined and the initial walking pattern is produced.

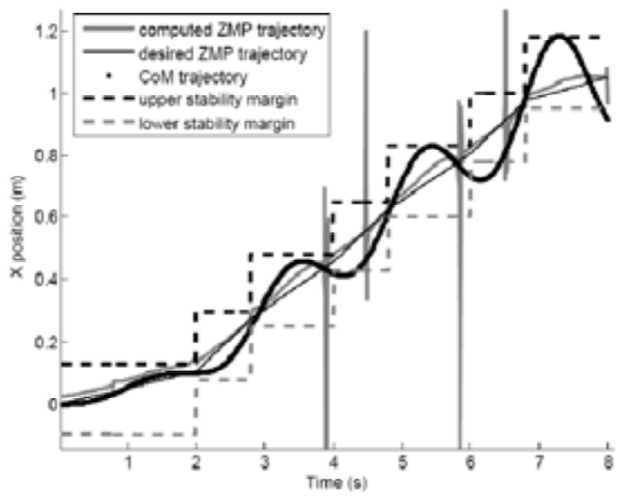

(a) Initial CoM trajectory

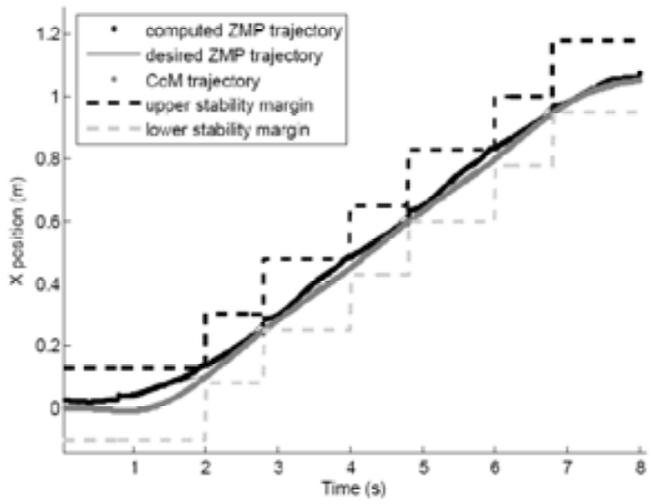

(b) Adjusted CoM trajectory

Fig. 16. Comparison between initial and adjusted CoM trajectories

4.3 Knee stretch motion

In human walking cycle, the knee angle reaches its minimum value during the heel strike motion (Perry, 1992). Here we introduce time parameters T_k, T_{ka} and T_{kb}, which mark the time when knee angle reach its minimum value, the beginning and ending time of the knee-stretch motion period. In this section we will explain how the knee-stretch motion is performed and how it can prevent the singularity.

4.3.1 Knee trajectory

After deciding the initial trajectory, the initial knee angle trajectory ($\theta_k(t)$) is modified during this knee-stretch period. Let (θ_{k1} and θ_{k2}) be the values of knee angle at $kT_k - T_{ka}$ and $kT_k - T_{kb}$, so that the new knee angle trajectory can be expressed as

$$\theta_k(t) = \begin{cases} \theta_{k1}, & t = kT_k - T_{ka} \\ 0, & t = kT_k \\ \theta_{k2}, & t = kT_k - T_{kb} \end{cases} \quad (21)$$

and the new continuous knee angle trajectory is obtained by cubic spline interpolation.

4.3.2 Inverse kinematic solution and singularity avoidance

The initial trajectory is obtained by specifying ankle trajectory and hip trajectory, and the knee trajectory is obtained by inverse kinematics solution. In sagittal plane, this scheme is exactly the same as 2 link planar mechanism, and if the knee angle is zero, the inverse kinematics solution will produce imaginary value known as singularity. In our algorithm, we will keep the hip trajectory as it is, and the ankle trajectory is modified as follows. During the time period of ($kT_k - T_{ka} < t < kT_k - T_{kb}$), instead of determining the knee position from the ankle and hip trajectories, we utilize the heel position and the modified knee angle trajectories to find the solution of knee and ankle position through the inverse kinematics problem. In this way, the system will become as three-link planar mechanism. As a result, the loss of the degree of freedom at the knee position can still be overcome by extra DOF at the heel joint. This can be explained as shown in Figure 17.

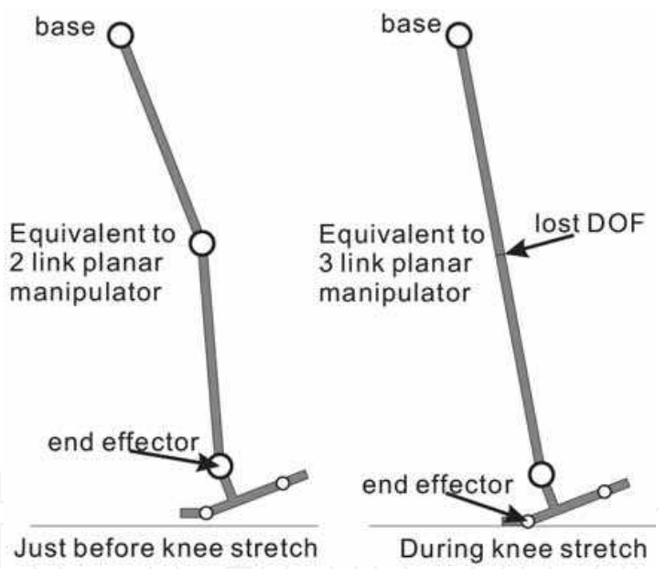

Fig. 17. Extra DOF at heel joint that avoid singularity.

After modifying the knee angle trajectory and obtaining modified parameters from previous steps, new knee and foot trajectories are obtained. The modification also changes the initial heel strike angle q_f. A complete algorithm description is shown in Figure 18.

4.4 Simulation result

The simulations have been performed in ADAMS. This simulation was intended to verify the effectiveness of the algorithm in terms of stability, torque requirements and energy consumptions. Comparisons have been done between the proposed gait pattern and a common gait pattern of the biped robot. The parameters of the biped robot (Figure 13) were

set according to Table I. The walking speed was 2 s/step with the step length of 0.35 m/step.

Figure 19 is for the stick figures and knee angle trajectories obtained from the algorithm. Both results were compared with those in human which indicates a similarity compared to common gait pattern. Although they do not perfectly match, it can be observed that the knee, foot and foot angle trajectories show quite similar trends to those in human. Figure 20 shows the comparison between the knee angle of biped robot and human in the same 100% walking cycle, though not all parts of the trajectory are the same, similarity can be seen in some period of time during the knee stretch motion and our proposed pattern can also generate 0^{o} knee angle. During around 40% of the walking cycle, which is at the toeoff motion, our proposed pattern is different from human. This was due to the fact that humans also generate an almost knee stretch motion during toe-off.

The knee stretch walking not only gives natural and humanlike walking pattern but also better performance in the knee torque requirement (Kurazume et al., 2005; Ogura et al., 2006). This gives an opportunity to employ smaller actuators for the knee. Figure 9 shows knee joint torque comparison between the common gait and the proposed gait, it is clearly shows that the proposed gait has less torque requirement. Figure 21 shows knee joint energy consumption comparison between the common gait and the proposed gait. The proposed gait shows better performance than the common gait. Table II summarize the torque requirement and energy consumption comparisons between the common gait and the proposed gait. All of the joint torque requirements of the proposed gait pattern is less than those in the common gait pattern. The addition of the heel and toe joints did not show high torque requirements, so it will make it possible for real implementation. In terms of energy consumptions, the overall result shows that the proposed gait pattern shows better performance compared to the common gait.

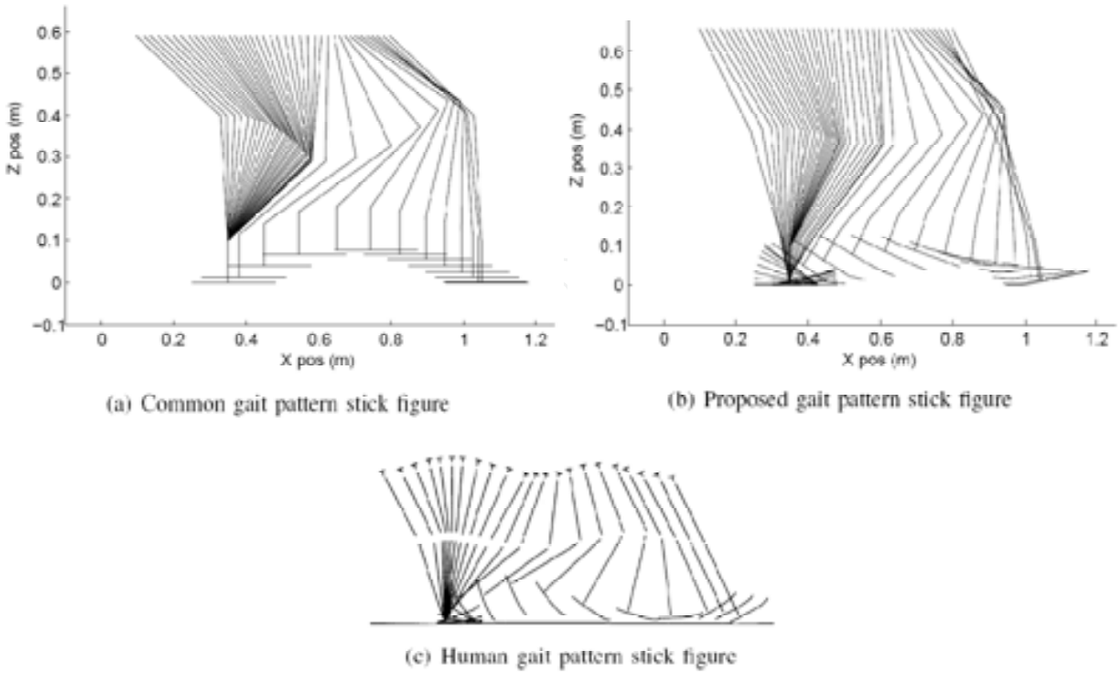

(a) Common gait pattern stick figure

(b) Proposed gait pattern stick figure

(c) Human gait pattern stick figure

Fig. 19. Stick figure comparison with human.

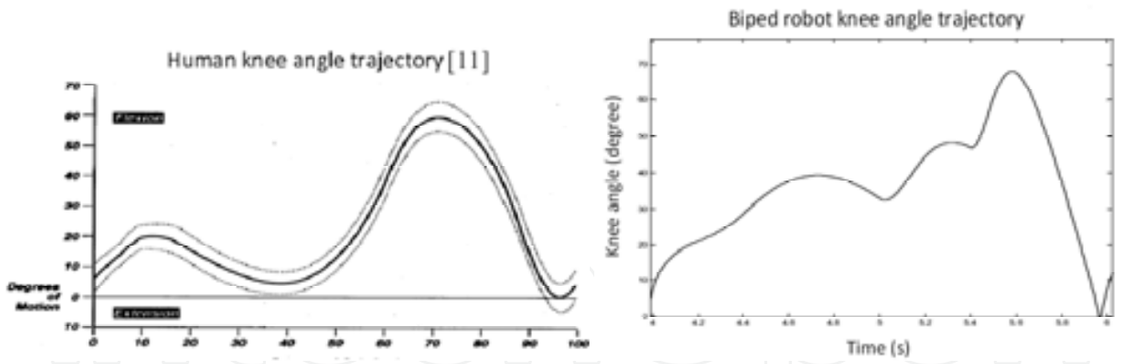

Fig. 20. Knee angle comparison with human.

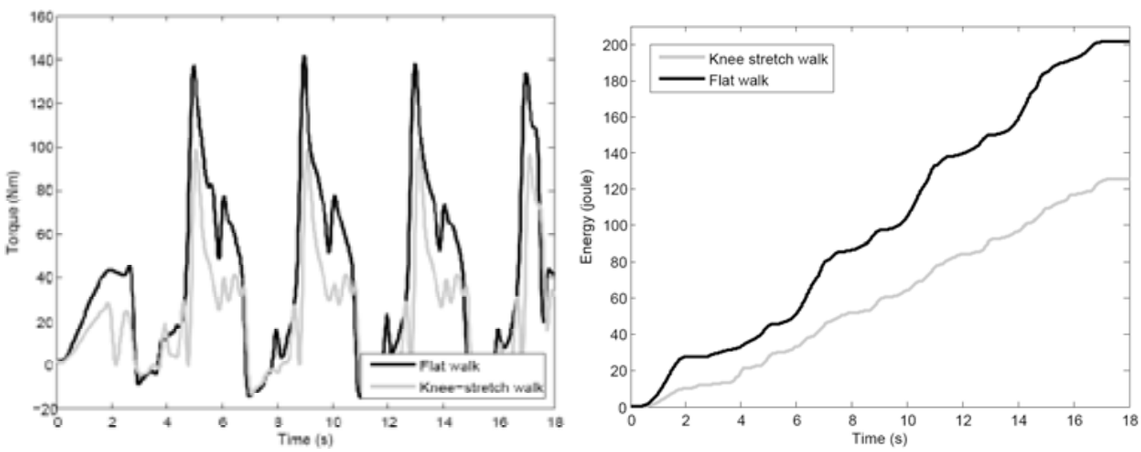

Fig. 21. Knee torque and energy consumption comparison between the common gait and the proposed gait.

Length (cm)	l_{tr}	l_{th}	l_{sh}	l_{an}	l_{ab}	l_{af}	l_{toe}	l_{heel}
	50	30	30	10	5	8	5	5
Weight(kg)	m_{tr}	m_{th}	m_{sh}	m_{foot}	m_{toe}	m_{heel}		
	43	10	5.7	2.5	0.3	0.3		
inertia(kgm^2)	I_{tr}	I_{th}	I_{sh}	I_{foot}	I_{toe}	I_{heel}		
	1.69	0.02	0.08	0.008	0.002	0.002		

Table I Parameters of The Biped Robot Model

	Joints	Common gait	Proposed gait
Torque Requirements (Nm)	hip	52.24	49.36
	knee	141.34	99.46
	ankle	75.19	69.13
	toe	-	14.42
	heel	-	19.62
	Joints	Common gait	Proposed gait
Energy Consumption (Joule)	hip	161.19	106.26
	knee	201.71	125.56
	ankle	72.39	133.24
	toe	-	21.29
	heel	-	6.19
	Total	435.29	392.54

Table II Summary of The Simulation Results

Figure 22 shows a frame by frame animation of the resulting algorithm. It can be noticed that the knee stretch occurs during the heel strike motion. The animation showed that the biped robot can walk stably without falling.

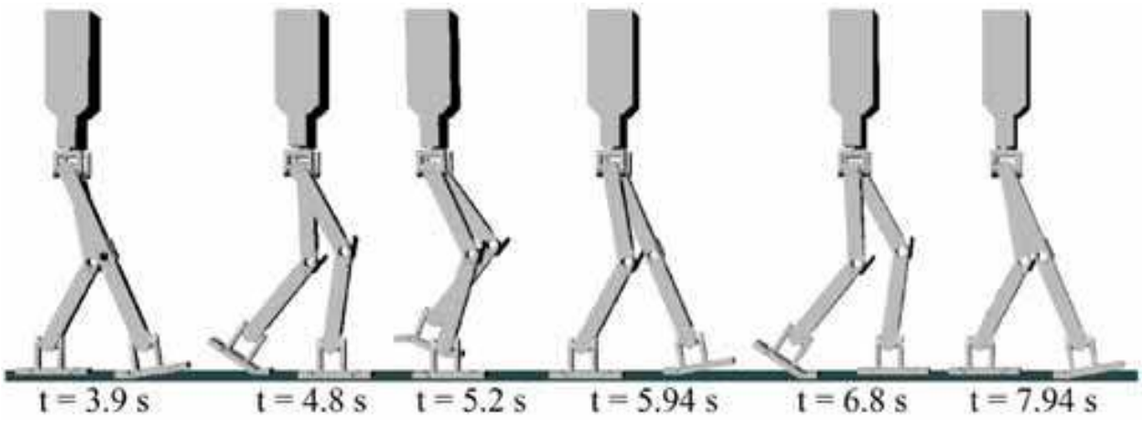

Fig. 22. Sequence of successive frame showing knee stretch walking pattern.

5. Conclusions

During walking sequence, human heels act as passive joints that create some support area, which helps the stability of human walking. This research attempts to replace human-heel like mechanism with heel joint in the biped robot foot. The existence of heel joints in the biped robot feet has two main advantages. The first one is that the support area during double support phase will be increased. Secondly, singularity during knee stretch motion can be avoided.

This chapter presents a new mechanism for toe&foot&heel motions with multi-platforms using a serial-parallel hybrid mechanism. The suggested mechanism can generate pitch and roll motions at ankle position, during toe and heel joint motions. These motions are adequate for natural foot and ankle movements of a humanoid robot. The developed foot device with the suggested mechanism will allow humanoid robots to walk more stably and in ways that are more natural. A new alternative method for generating knee stretch walking pattern for biped robot utilizing toe and heel joints has been also presented with this chapter, which has several advantages over previous algorithms. The proposed algorithm was verified using computer simulation, and better performances have been obtained as compared to common gait pattern. The improvements for the effectiveness of the proposed algorithm in terms of joint torque requirements as well as energy consumptions have been presented.

It is observed that the utilization of toe and heel joints increases the stability margin during the double support phase, thus giving more freedom in designing the walking patterns. Furthermore, the addition of heel joint has the advantage of avoiding singularity during the knee stretch motion, because the loss of degree of freedom in the knee can still be compensated by the existence of extra dof in the heel joint. While the previous researchers have also suggested the addition of waist joint to avoid singularity, compared to waist joint, two heel joints are comparably smaller and less complicated. For existing biped robots, it will be a lot easier to modify the foot than to modify the waist. As a final point, the pattern

obtained from this method shows similarities with those of human walking pattern, thus can provide more natural walking for the robot.

6. Acknowledgment

This work was supported in part by the Korea Research Foundation funded by the Korean Government (Ministry of Education and Human Resources Development) under Grant KRF-2008- 331-D00027 and in part by the Priority Research Centers Program through the National Research Foundation of Korea funded by the Ministry of Education, Science and Technology under Grant 2009-0094016.

7. References

Ahn C.; Lee, M.; Go, S. (2003). Development of a biped robot with toes to improve gait pattern, *Proc. of the IEEE/ASME Int. Conf. on Advanced Intelligent Mechatronics (AIM2003*), pp729-734.

Choi,Y; Kim, D; Oh, Y. & You, B.J. (2007). Posture/ Walking Control for Humanoid Robot Based on Kinematic Resolution of CoM Jacobian With Embedded Motion, IEEE Trans. on Robotics, vol. 23, no. 6, pp. 1285-1293.

Guihard, M. & Gorce, P. (2004). Biorobotic foot model applied to BIPMAN robot, IEEE International Conference on Systems, Man and Cybernetics, pp6491-6496.

Huang, Q.; Yokoi,K.; Kajita, S.; Kaneko, K.; Arai, H.; Koyachi, N.; Tanie, K. (2001). Planning Walking Patterns for a Biped Robot, IEEE Trans. on Robotics and Automation, vol.17, no.3, pp. 280-289.

Ki Ahn, C.; Cheol Lee, M.; Jo Go, S. (2003). Development of a Biped Robot with Toes to Improve Gait Pattern, Proceedings of the IEE/ASME International Conference on Advanced Intelligent Mechatronics.

Kurazume, R.; Tanaka, S; Yamasi, M; Hasegawa, T.; Yoneda, K. (2005) Straight Legged Walking of a Biped Robot, in Proc. of the IEEE/RSJ International Conference on Intelligent Robots and Systems, Alberta, Canada, pp. 3095-3101 .

Nishiwaki, K. & Kagami, S. (2002). Toe joint that enhances bipedal and full body motion, IEEE Int. Conf. on Rob. and Auto.(ICRA 2002), pp3105-3110.

Nishiwaki, K.; Kagami, S.; Kuniyoshi, Y.; Inaba, M.; Inoue, H. (2002). Online Generation of Humanoid Walking Motion Based on a Fast Generation Method of Motion Patterns that Follows Desired ZMP, Proc. of the IEEE/RSJ International Conference on Intelligent Robots and Systems, Lausanne, Switzerland, October 2002, pp. 2684.

Nishiwaki, K.; Kagami, S.; Kuniyoshi, Y.; Inaba, M.; Inoue, H. (2002). Toe Joints that Enhance Bipedal and Fullbody Motion of Humanoid Robots, Proc. of the IEEE International Conference on Robotics & Automation, Washington, DC.

Ogura, Y.; Lim, H & Takanishi, A. (2003) Stretch Walking Pattern Generation for a Biped Humanoid Robot, in Proc. of the IEEE/RSJ International Conference on Intelligent Robots and Systems, Las Vegas, USA, pp. 352-357.

Ogura, Y.; Shimomura, K.; Kondo, H; Morishima, A.; Okubo, T; Momoki S.; Lim, H.; Takanishi, A. (2006). Humanlike Walking with Knee Stretched, Heel-contact and

Toe-off Motion by a Humanoid Robot, in Proc. of the IEEE/RSJ International Conference on Intelligent Robots and Systems, Beijing, China, pp. 3976-3981.

Okada, K.; Ogura, T.; Haneda, A.; Kousaka, D.; Nakai, H.; Inaba, M.; Inoue, H. (2004). Integrated System Software for HRP2 Humanoid, Proceedings of the 2004 IEEE International Conference on Robotics & Automation, New Orleans, LA.

Peng Z.; Huang, Q.; Zhao, X.; Xiao, T.; Li, K. (2004). Online Trajectory Generation Based on off-line Trajectory for Biped Humanoid, Proceedings of the 2004 IEEE International Conference on Robotics and Biomimetics, Shenyang, China, August 2004, pp. 752.

Perry, J. (1992). Gait Analysis:Normal and Pathological Function , Slack Inc., Thorofare, N. J., 1992.

R. Garage, (2008) http://www.robogarage. com/english/robo/chroino.html.

Ramzi, S.; Olivier, S.; Shuuji, Kajita; Kazuhito, Y. & Abderrahmane, K. (2006). Faster and Smoother Walking of Humanoid HRP-2 with Passive Toe Joints, Proc. of the IEEE/RSJ International Conference on Intelligent Robots and Systems, Beijing, China, pp. 4909- 4914.

Sakagami, Y.; Watanabe R.; Aoyama C.; Matsunaga S.; Higaki N.; Fujimura K. (2002). The intelligent ASIMO : System Overview and Integration, Proceedings of the 2002 IEEE/RSJ Intl. Conference on Intelligent Robots and Systems EPFL, Lausanne, Switzerland.

Takahashi, T. & Kawamura, A. (2204) Posture control using foot toe and sole for biped walking robot Ken, AMC, Maribor, Slovenica, pp.437-442.

Takao, S; Ohta, H.; Yokokohji, Y.; Yoshikawa, T. (2004). Function analysis of human-like mechanical foot, using mechanically constrained shoes, IEEE/RSJ Int. Conf. on Intelligent Robots and System (IROS2004), pp3847-3852.

www.mathworks.com

Yoon, J. W.; Handharu, N.; Kim, G.S. (2007). A Bio-Robotic Toe and Foot and Heel Models of a Biped Robot for More Natural Walking, Proc. Of The IASTED International Conference on Modeling, Identification & Control, Innsbruck, Austria.

Biped Robots

Edited by Prof. Armando Carlos Pina Filho

ISBN 978-953-307-216-6
Hard cover, 322 pages
Publisher InTech
Published online 04, February, 2011
Published in print edition February, 2011

Biped robots represent a very interesting research subject, with several particularities and scope topics, such as: mechanical design, gait simulation, patterns generation, kinematics, dynamics, equilibrium, stability, kinds of control, adaptability, biomechanics, cybernetics, and rehabilitation technologies. We have diverse problems related to these topics, making the study of biped robots a very complex subject, and many times the results of researches are not totally satisfactory. However, with scientific and technological advances, based on theoretical and experimental works, many researchers have collaborated in the evolution of the biped robots design, looking for to develop autonomous systems, as well as to help in rehabilitation technologies of human beings. Thus, this book intends to present some works related to the study of biped robots, developed by researchers worldwide.

InTech Europe
University Campus STeP Ri
Slavka Krautzeka 83/A
51000 Rijeka, Croatia
Phone: +385 (51) 770 447
Fax: +385 (51) 686 166
www.intechopen.com

InTech China
Unit 405, Office Block, Hotel Equatorial Shanghai
No.65, Yan An Road (West), Shanghai, 200040, China
中国上海市延安西路65号上海国际贵都大饭店办公楼405单元
Phone: +86-21-62489820
Fax: +86-21-62489821

IntechOpen